Supporting Information

Quasi-1D Mn_2O_3 Nanostructures Functionalized with First-Row Transition Metal Oxides as Oxygen Evolution Catalysts

Lorenzo Bigiani,[†] Chiara Maccato,*,[†] Teresa Andreu,[§,||] Alberto Gasparotto,[†] Cinzia Sada,[#]

Evgeny Modin,[⊥] Oleg I. Lebedev,[▽] Joan Ramon Morante,[§,||] and Davide Barreca[‡]

[†] Department of Chemical Sciences, Padova University and INSTM, 35131 Padova, Italy

[§] IREC, Catalonia Institute for Energy Research, 08930 Sant Adrià de Besòs, Barcelona, Catalonia, Spain

[||] Universitat de Barcelona (UB), 08028 Barcelona, Spain

[#] Department of Physics and Astronomy, Padova University and INSTM, 35131 Padova, Italy

[⊥] CIC nanoGUNE BRTA, 20018 Donostia - San Sebastian, Spain

[▽] Laboratoire CRISMAT, ENSICAEN UMR6508, 14050 Caen Cedex 4, France

[‡] CNR-ICMATE and INSTM, Department of Chemical Sciences, Padova University, 35131 Padova, Italy

* Corresponding author; E-mail: chiara.maccato@unipd.it

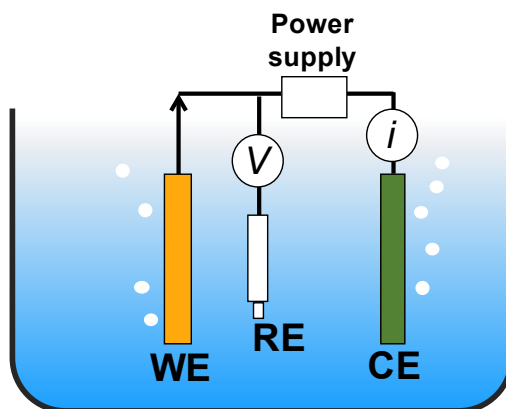# § S1. Chemico-Physical Characterization

Figure S1. Sketch of the electrochemical experimental setup. WE, RE, and CE represent working electrode (Ni foam-supported specimens), reference electrode (Hg/HgO), and counter electrode (Pt mesh), respectively.
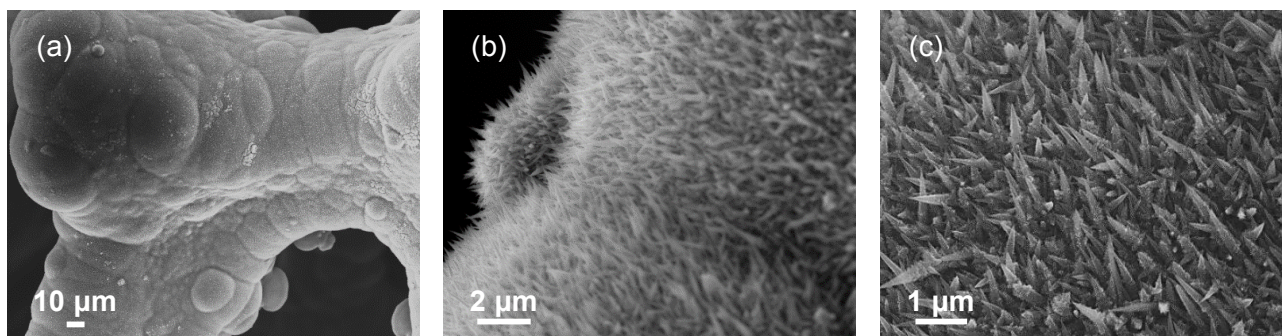

Figure S2. (a-c) Field emission-scanning electron microscopy (FE-SEM) micrographs at different magnification levels for bare Mn_2O_3 on Ni foam.
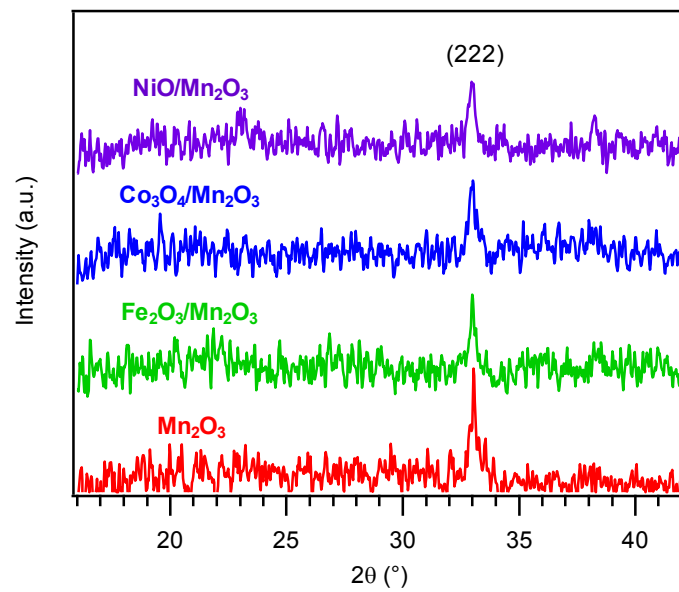
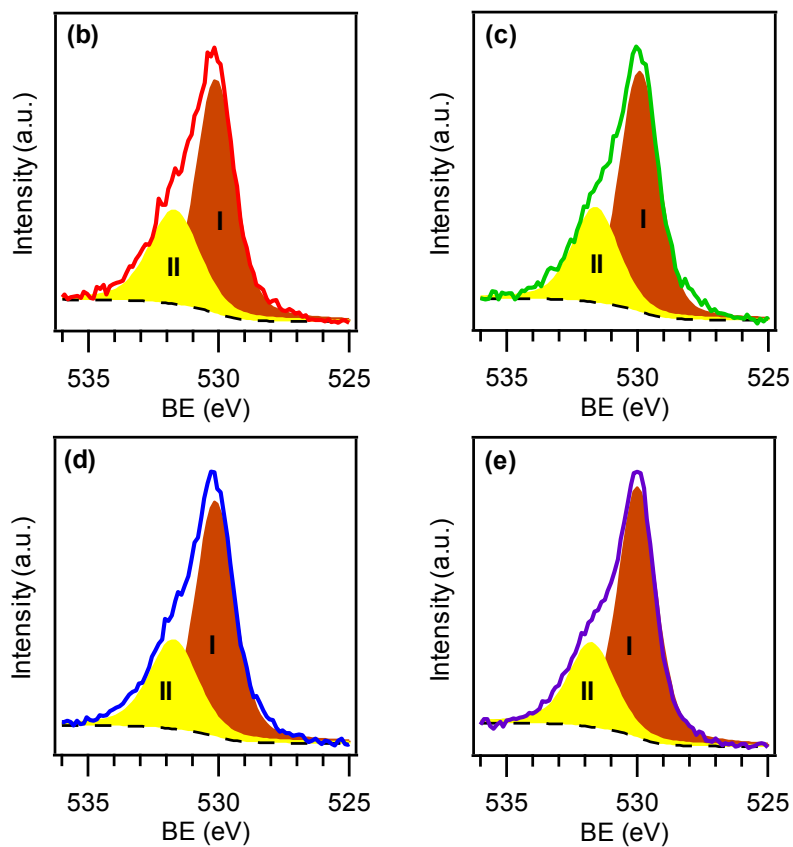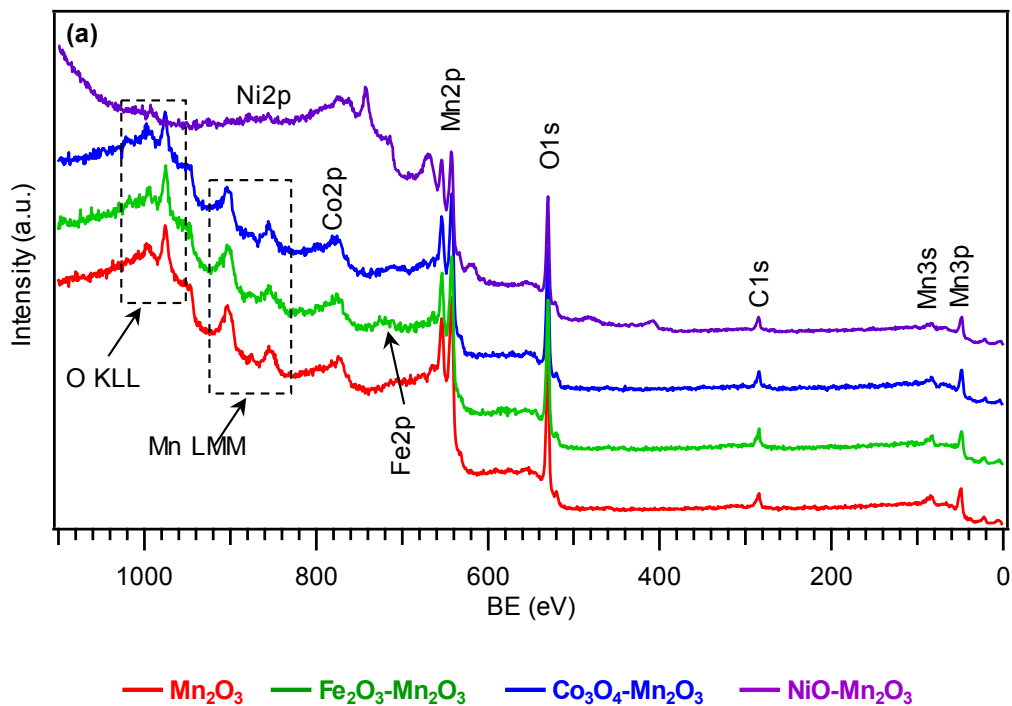**Figure S3.** X-ray diffraction (XRD) patterns for Mn_2O_3-based specimens deposited on Ni foams.

Figure S4. (a) Surface X-ray photoelectron spectroscopy (XPS) surveys of Mn_2O_3-based electrodes. O1s photoelectron peaks, along with the resulting fitting components, for Mn_2O_3 (b), Fe_2O_3-Mn_2O_3 (c), Co_3O_4-Mn_2O_3 (d), and NiO-Mn_2O_3 (e).
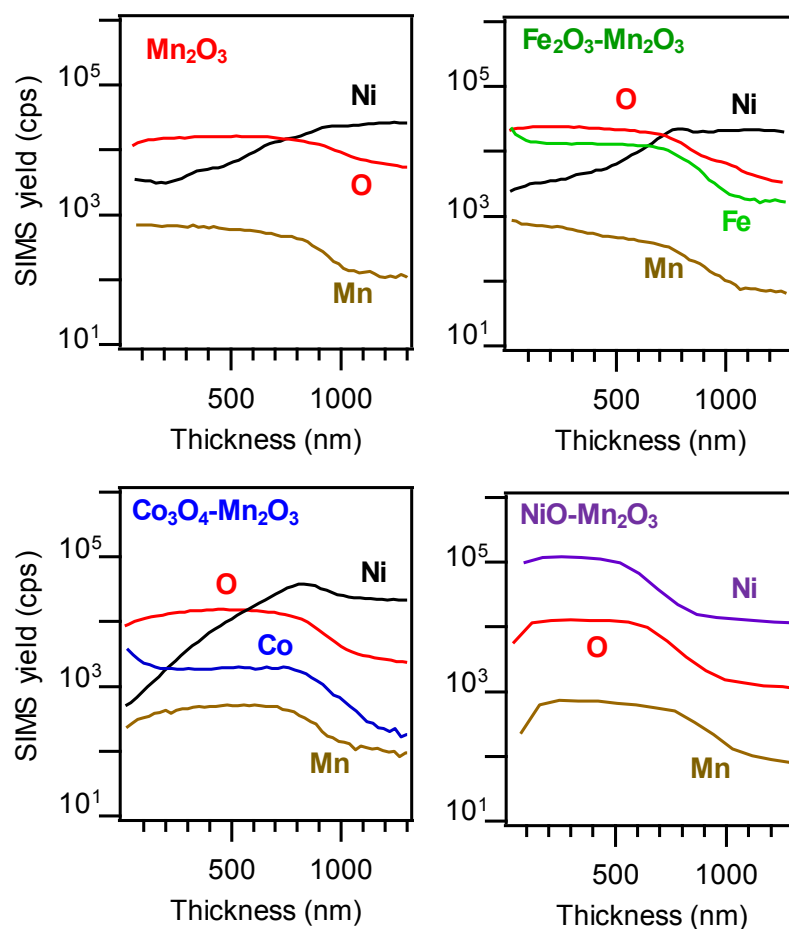
Figure S5. Secondary ion mass spectrometry (SIMS) depth profiles for the target samples.

In-depth compositional analyses by SIMS (Figure S4) revealed a good purity of the target materials (average C concentration < 100 ppm). In all cases, manganese and oxygen ionic yields were almost parallel throughout the investigated depth, a feature evidencing their common chemical origin. The trend of M (M = Fe, Co, Ni) signal as a function of thickness indicated that the functionalizing agents were present even in the inner regions of Mn_2O_3 network. This phenomenon was attributed to the synergy between the porous structure of Ni foam-supported Mn_2O_3 and the inherent RF-Sputtering infiltration power,[1-2] which was also the main origin of the broad deposit/substrate interface.

§ S2. Electrochemical Tests

Material	Electrolyte	j @ 1.65 V (mA/cm^2)	η @ 10 mA/cm^2 (mV)	Tafel slope (mV/decade)	Ref.
Ni foam	1.0 M KOH	4.0	477	99	Present work
Mn$_2$O$_3$		20	379	93	
Fe$_2$O$_3$-Mn$_2$O$_3$		32	352	71	
Co$_3$O$_4$-Mn$_2$O$_3$		24	360	95	
NiO-Mn$_2$O$_3$		26	361	84	
Mn$_3$O$_4$	1.0 M NaOH	4	501	107	3
Mn$_3$O$_4$		10	421	121	
Mn$_5$O$_8$		5	481	108	
Mn$_2$O$_3$		18	351	99	
Mn$_2$O$_3$	0.1 M KOH	5	511	128	4
MnO$_2$	0.1 M KOH	2	570	152	5
MnO$_2$-CoFe$_2$O$_4$/C	0.1 M KOH	6	471	130	6
Li-MnO$_x$	0.1 M KOH	4	521	231	7
MnO$_2$-Mn$_2$O$_3$	1.0 M KOH	10	421	109	8
Mn$_{0.8}$Ru$_{0.2}$O$_2$	0.1 M KOH	12	411	86	9
Co doped MnO$_2$	0.1 M KOH	3	491	73	10
Mn$_2$O$_3$	1.0 M NaOH	2	601	130	11
RuO$_2$-Mn$_2$O$_3$		15	371	70	
Mn$_2$O$_3$	0.1 M KOH	10	421	81	12
Mn$_3$O$_4$		5	491	95	
Mn$_2$O$_3$	1.0 M KOH	60	291	85	13

Table S1. Comparison of oxygen evolution reaction (OER) performances of the actual Mn$_2$O$_3$-based materials with selected literature data reported for manganese oxide electrocatalysts operating in alkaline media.

Material	Electrolyte	j @ 1.65 V (mA/cm²)	E @ 10 mA/cm² (V vs RHE)	Tafel slope (mV/decade)	Ref.
IrO$_2$	1.0 M KOH	65	331	62	14
IrO$_2$	1.0 M KOH	50	331	54	15
IrO$_2$	1.0 M KOH	18	391	149	16
IrO$_2$	1.0 M KOH	53	321	91	17
IrO$_2$	0.1 M KOH	8	461	113	12
IrO$_2$	1.0 M KOH	27	351	67	18
RuO$_2$		15	371	89	
RuO$_2$	0.1 M KOH	17	391	71	19
RuO$_2$	0.1 M KOH	52	301	62	20
RuO$_2$	1.0 M KOH	13	411	74	21

Table S2. OER performances of selected IrO$_2$ and RuO$_2$ electrocatalysts operating in alkaline media.
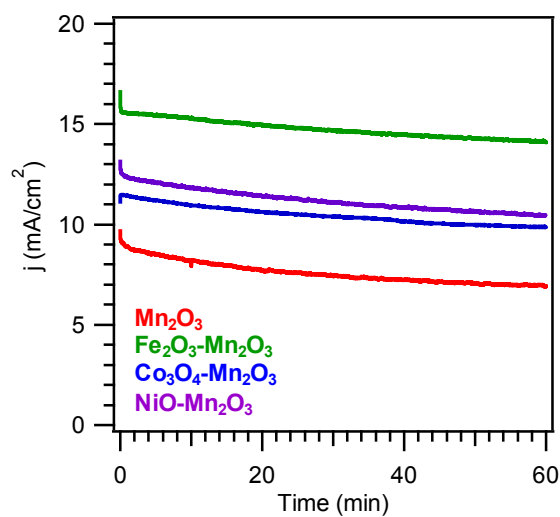

Figure S6. Chronoamperometry curves for the target specimens at a fixed potential of 1.60 V *vs.* the reversible hydrogen electrode (RHE).
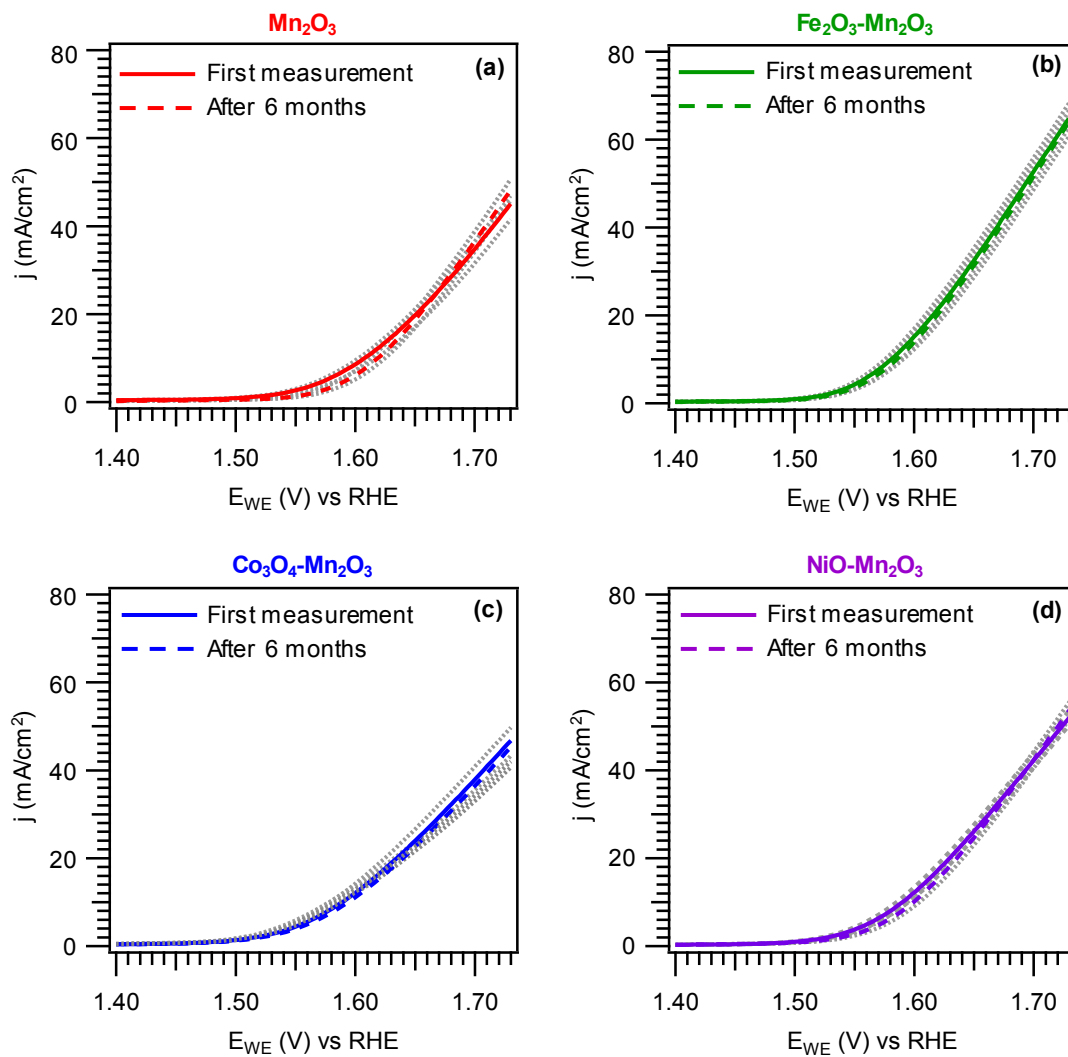
Figure S7. Linear sweep voltammetry (LSV) curves collected on as-prepared samples (solid line) and after 6 months (dashed line) for (a) Mn_2O_3, (b) Fe_2O_3-Mn_2O_3, (c) Co_3O_4-Mn_2O_3, and (d) NiO-Mn_2O_3. Grey curves represent LSV data recorded monthly over a period of 6 months.
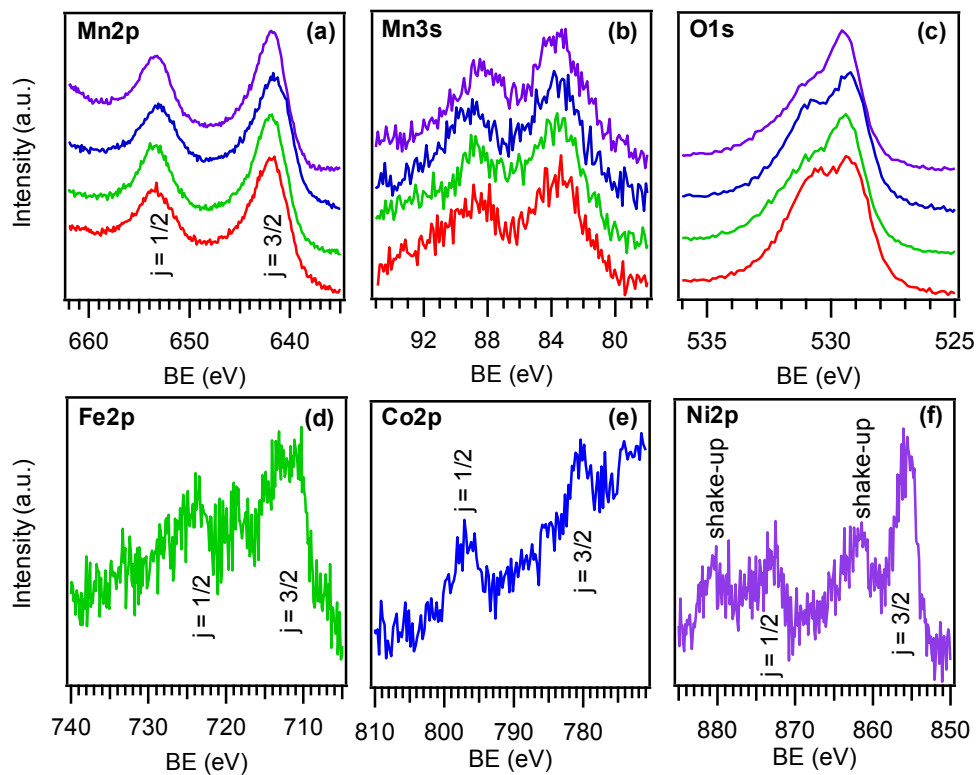
Figure S8. XPS spectra of (a) Mn2p, (b) Mn3s, (c) O1s, (d) Fe2p, (e) Co2p, (f) Ni2p for Mn_2O_3-based electrodes after 6 months.

References

(1) Carraro, G.; Gasparotto, A.; Maccato, C.; Bontempi, E.; Bilo, F.; Peeters, D.; Sada, C.; Barreca, D. A Plasma-Assisted Approach for the Controlled Dispersion of CuO Aggregates into β Iron(III) Oxide Matrices. *CrystEngComm* **2014**, *16*, 8710-8716.

(2) Carraro, G.; Maccato, C.; Gasparotto, A.; Kaunisto, K.; Sada, C.; Barreca, D. Plasma-Assisted Fabrication of Fe_2O_3-Co_3O_4 Nanomaterials as Anodes for Photoelectrochemical Water Splitting. *Plasma Processes Polym.* **2016**, *13*, 191-200.

(3) Liu, G. Y.; Hall, J.; Nasiri, N.; Gengenbach, T.; Spiccia, L.; Cheah, M. H.; Tricoli, A. Scalable Synthesis of Efficient Water Oxidation Catalysts: Insights into the Activity of Flame-Made Manganese Oxide Nanocrystals. *ChemSusChem* **2015**, *8*, 4162-4171.

(4) Jahan, M.; Tominaka, S.; Henzie, J. Phase Pure α-Mn_2O_3 Prisms and their Bifunctional Electrocatalytic Activity in Oxygen Evolution and Reduction Reactions. *Dalton Trans.* **2016**, *45*, 18494-18501.

(5) He, J.; Wang, M.; Wang, W.; Miao, R.; Zhong, W.; Chen, S.-Y.; Poges, S.; Jafari, T.; Song, W.; Liu, J.; Suib, S. L. Hierarchical Mesoporous NiO/MnO_2@PANI Core–Shell Microspheres, Highly Efficient and Stable Bifunctional Electrocatalysts for Oxygen Evolution and Reduction Reactions. *ACS Appl. Mater. Interfaces* **2017**, *9*, 42676-42687.

(6) Wang, Y.; Liu, Q.; Hu, T.; Zhang, L.; Deng, Y. Carbon Supported MnO_2-$CoFe_2O_4$ with Enhanced Electrocatalytic Activity for Oxygen Reduction and Oxygen Evolution. *Appl. Surf. Sci.* **2017**, *403*, 51-56.

(7) Kosasang, S.; Ma, N.; Wuamprakhon, P.; Phattharasupakun, N.; Maihom, T.; Limtrakul, J.;

Sawangphruk, M. Insight into the Effect of Intercalated Alkaline Cations of Layered Manganese Oxides on the Oxygen Reduction Reaction and Oxygen Evolution Reaction. *Chem. Commun.* **2018**, *54*, 8575-8578.

(8) Liu, P.-P.; Li, T.-T.; Zhu, H.-L.; Zheng, Y.-Q. Manganese Oxide with Hollow Rambutan-Like Morphology as Highly Efficient Electrocatalyst for Oxygen Evolution Reaction. *J. Solid State Electrochem.* **2018**, *22*, 2999-3007.

(9) Kang, B.; Jin, X.; Oh, S. M.; Patil, S. B.; Kim, M. G.; Kim, S. H.; Hwang, S.-J. An Effective Way to Improve Bifunctional Electrocatalyst Activity of Manganese Oxide via Control of Bond Competition. *Appl. Catal., B* **2018**, *236*, 107-116.

(10) West, P. J.; Byles, B. W.; Pomerantseva, E. Creation of Controllable Cationic and Anionic Defects in Tunnel Manganese Oxide Nanowires for Enhanced Oxygen Evolution Reaction. *Polyhedron* **2019**, *171*, 32-40.

(11) Browne, M. P.; Nolan, H.; Twamley, B.; Duesberg, G. S.; Colavita, P. E.; Lyons, M. E. G. Thermally Prepared $Mn_2O_3/RuO_2/Ru$ Thin Films as Highly Active Catalysts for the Oxygen Evolution Reaction in Alkaline Media. *ChemElectroChem* **2016**, *3*, 1847-1855.

(12) Sim, H.; Lee, J.; Yu, T.; Lim, B. Manganese Oxide with Different Composition and Morphology as Electrocatalyst for Oxygen Evolution Reaction. *Korean J. Chem. Eng.* **2018**, *35*, 257-262.

(13) Liu, P.-P.; Zheng, Y.-Q.; Zhu, H.-L.; Li, T.-T. Mn_2O_3 Hollow Nanotube Arrays on Ni Foam as Efficient Supercapacitors and Electrocatalysts for Oxygen Evolution Reaction. *ACS Appl. Nano Mater.* **2019**, *2*, 744-749.

(14) Qin, F.; Zhao, Z.; Alam, M. K.; Ni, Y.; Robles-Hernandez, F.; Yu, L.; Chen, S.; Ren, Z.; Wang, Z.; Bao, J. Trimetallic NiFeMo for Overall Electrochemical Water Splitting with a Low Cell

Voltage. *ACS Energy Lett.* **2018**, *3*, 546-554.

(15) Yu, M. Q.; Jiang, L. X.; Yang, H. G. Ultrathin Nanosheets Constructed $CoMoO_4$ Porous Flowers with High Activity for Electrocatalytic Oxygen Evolution. *Chem. Commun.* **2015**, *51*, 14361-14364.

(16) Jiao, L.; Zhou, Y.-X.; Jiang, H.-L. Metal–Organic Framework-Based CoP/Reduced Graphene Oxide: High-Performance Bifunctional Electrocatalyst for Overall Water Splitting. *Chem. Sci.* **2016**, *7*, 1690-1695.

(17) Qazi, U. Y.; Yuan, C.-Z.; Ullah, N.; Jiang, Y.-F.; Imran, M.; Zeb, A.; Zhao, S.-J.; Javaid, R.; Xu, A.-W. One-Step Growth of Iron–Nickel Bimetallic Nanoparticles on FeNi Alloy Foils: Highly Efficient Advanced Electrodes for the Oxygen Evolution Reaction. *ACS Appl. Mater. Interfaces* **2017**, *9*, 28627-28634.

(18) Xiao, Q.; Zhang, Y.; Guo, X.; Jing, L.; Yang, Z.; Xue, Y.; Yan, Y.-M.; Sun, K. A High-Performance Electrocatalyst for Oxygen Evolution Reactions based on Electrochemical Post-Treatment of Ultrathin Carbon Layer Coated Cobalt Nanoparticles. *Chem. Commun.* **2014**, *50*, 13019-13022.

(19) Ahmed, M. S.; Choi, B.; Kim, Y.-B. Development of Highly Active Bifunctional Electrocatalyst Using Co_3O_4 on Carbon Nanotubes for Oxygen Reduction and Oxygen Evolution. *Sci. Rep.* **2018**, *8*, 2543.

(20) Li, X.; Wang, H.; Cui, Z.; Li, Y.; Xin, S.; Zhou, J.; Long, Y.; Jin, C.; Goodenough, J. B. Exceptional Oxygen Evolution Reactivities on $CaCoO_3$ and $SrCoO_3$. *Sci. Adv.* **2019**, *5*, eaav6262.

(21) Das, D.; Das, A.; Reghunath, M.; Nanda, K. K. Phosphine-Free Avenue to Co_2P Nanoparticle Encapsulated N,P co-Doped CNTs: A Novel Non-Enzymatic Glucose Sensor and an Efficient

Electrocatalyst for Oxygen Evolution Reaction. *Green Chem.* **2017**, *19*, 1327-1335.